

Supporting information for

## **Endogenous Metal-Ion Dynamic Nuclear Polarization for NMR Signal Enhancement in Metal Organic Frameworks**

Ilia B. Moroz<sup>a</sup>, Yishay Feldman<sup>b</sup>, Raanan Carmieli<sup>b</sup>, Xinyu Liu<sup>c</sup> and Michal Leskes<sup>a\*</sup>

<sup>a</sup>Department of Molecular Chemistry and Materials Science, Weizmann Institute of Science, Rehovot 76100, Israel

<sup>b</sup>Department of Chemical Research Support, Weizmann Institute of Science, Rehovot 76100, Israel

<sup>c</sup>Yusuf Hamied Department of Chemistry, University of Cambridge, Lensfield Road, Cambridge, CB12 1EW, UK

\*Corresponding author

Email: michal.leskes@weizmann.ac.il

### Contents

<b>General Materials and Methods .....</b>	<b>2</b>
<b>Materials and Gd-LaBTB synthesis .....</b>	<b>2</b>
<b>Introduction of ethylene glycol into Gd-LaBTB.....</b>	<b>3</b>
<b>X-ray powder diffraction (XRD).....</b>	<b>3</b>
<b>Energy Dispersive X-Ray Fluorescence (EDXRF) spectroscopy .....</b>	<b>3</b>
<b>FTIR spectroscopy .....</b>	<b>3</b>
<b>EPR measurements.....</b>	<b>4</b>
<b>NMR measurements .....</b>	<b>4</b>
<b>“Freeze-thaw” protocol .....</b>	<b>4</b>
<b>Additional experimental data.....</b>	<b>5</b>
<b>References .....</b>	<b>25</b>

## General Materials and Methods

### Materials and Gd-LaBTB synthesis

1,3,5-Benzenetribenzoic acid or H<sub>3</sub>BTB (97% purity, Holland Moran), lanthanum nitrate hexahydrate (99.99%, Holland Moran), gadolinium nitrate hexahydrate (99.9%, Tzamal D-Chem), NaOH (99.99%, Holland Moran) cyclohexanol (99%, Merck), dimethylformamide (DMF, 99.8%, Thermoscientific), tetrahydrofuran (THF, >99.9%, inhibitor-free, Sigma Aldrich), ethylene glycol (EG, >99.5%, Bio-Lab Ltd.) were purchased from respective vendors and used without further purification. Gd(III)-doped LaBTB samples, where BTB is benzenetribenzoate linker, were synthesized according to the modified literature procedure.<sup>1</sup> Gd<sub>x</sub>-LaBTB: 179.7 mg (0.415 mmol) of La(NO<sub>3</sub>)<sub>3</sub>·6H<sub>2</sub>O, *y* mg of Gd(NO<sub>3</sub>)<sub>3</sub>·6H<sub>2</sub>O (where *y* corresponds to Gd:La atomic ratio *x* of 0, 0.0011, 0.0021, 0.0042, 0.0084 and 0.0167) and 1 equiv. of H<sub>3</sub>BTB with respect to the total metal amount (ca. 182 mg) were placed in a 45 mL Teflon-lined steel autoclave. Water (Millipore, 4.5 mL) and 0.36 mL of 2M NaOH solution were added to the autoclave, and the obtained slurry was stirred for 2 mins. Next 4.5 mL of liquid cyclohexanol (ca. 313 K) were added, and the mixture was stirred for another 10 mins. The autoclave was then sealed, placed in an oven preheated to 373 K and kept at this temperature for 5 days. The white solid product was separated by centrifugation, washed with ethanol (40 mL), water (30 mL), ethanol (2×40 mL), methanol (45 mL) and dried in air at 353 K (as-synthesized materials). The activated samples were obtained by heating the as-synthesized products at 423 K for 16 h under vacuum (ca. 10<sup>-1</sup> mbar) and stored in an Ar-filled glovebox prior to characterization.

An alternative synthetic route was a modification of the literature procedure described by Kitagawa and co-workers.<sup>2</sup> 108.3 mg (0.25 mmol) of La(NO<sub>3</sub>)<sub>3</sub>·6H<sub>2</sub>O, *y* mg of Gd(NO<sub>3</sub>)<sub>3</sub>·6H<sub>2</sub>O (where *y* corresponds to Gd:La atomic ratio *x* of 0, 0.0011, 0.0033, and 0.0099) and 0.34 equiv. of H<sub>3</sub>BTB with respect to the total metal amount (ca. 37.3 mg) were placed in a 45 mL Teflon-lined steel autoclave. A mixture of 3DMF:3CH<sub>3</sub>OH:1H<sub>2</sub>O with a total volume of 12.5 mL was added to it and stirred for 4 hours. The autoclave was then sealed, placed in an oven preheated to 353 K and kept at this temperature for 2 days. The white solid product was separated by centrifugation, washed with ethanol (2×35 mL), methanol (5×35 mL) and dried in air at 353 K (as-synthesized materials). The activated samples were obtained by heating the as-synthesized products at 423 K for 16 h under vacuum (ca. 10<sup>-1</sup> mbar) and stored in an Ar-filled glovebox prior to characterization. This synthetic route led to formation of an impurity phase – lanthanum formate – together with the targeted LaBTB phase.

### **Introduction of ethylene glycol into Gd-LaBTB**

Ethylene glycol was loaded into Gd-LaBTB by incipient wetness impregnation of the MOF (20 mg) with a solution of ethylene glycol in THF, containing 1 equiv. of ethylene glycol with respect to metal in Gd-LaBTB, under inert atmosphere at ambient temperature. After 16 h, the powder was dried at ambient temperature for 2 h under vacuum (ca.  $10^{-1}$  mbar) to remove the excess of THF and stored in an Ar-filled glovebox prior to characterization.

### **X-ray powder diffraction (XRD)**

X-ray powder diffraction data of the as-synthesized Gd(x)-LaBTB samples were collected on a TTRAX-III (Rigaku, Japan) diffractometer equipped with a rotating Cu anode ( $\lambda = 1.5418 \text{ \AA}$ ) operating at 50 kV and 200 mA. The X-ray angle  $2\theta$  was scanned from 3 to 50 degrees with a step size of 0.02 degrees and a scan speed of 2 degrees per min. The activated samples were measured in reflection geometry on a SmartLab (Rigaku, Japan) diffractometer equipped with a rotating Cu anode operating at 45 kV and 200 mA. Materials were loaded into a cell covered with an X-ray transparent film inside an Ar-filled glovebox, and XRD patterns were collected without exposing samples to air.  $2\theta/\theta$  scans were performed at specular conditions in 1D detector mode with variable divergence and scattering slits, as well as a 5 mm receiving slit. The  $2\theta$  angle was scanned from 3 to 85 degrees with a step size of 0.02 degrees and a scan speed of 1 degree per minute.

### **Energy Dispersive X-Ray Fluorescence (EDXRF) spectroscopy**

EDXRF measurements were performed on a Genius-IF X-ray spectrometer (Xenometrix, Israel) equipped with a sealed Rh anode X-ray tube operating at 25 kV and 0.3 mA and a Silicon Drift Detector (SDD) with a high-count rate and resolution of 125 eV. The measurements were carried out in air for 10 minutes. To increase the detection sensitivity, a Ti filter was used, which had an appropriate absorption edge for the L lines of La and Gd.

### **FTIR spectroscopy**

Infrared spectra were recorded on an FTIR spectrometer Nicolet iS50 with an attenuated total reflection (ATR) accessory (Thermo Scientific). For each spectrum, 32 scans with resolution of  $4 \text{ cm}^{-1}$  were collected and the atmospheric background spectrum was subtracted. MOF samples were exposed to air for less than 5 mins prior to the measurement.

### **CO<sub>2</sub> adsorption-desorption isotherms**

The CO<sub>2</sub> gas sorption measurements were carried out using a high vacuum physisorption/chemisorption analyser (Autosorb iQ from Anton Paar) at 298 K. Both samples were degassed at 423 K in vacuo with a ramp of  $5 \text{ }^\circ\text{C}/\text{min}$  for 20 hours in 9 mm glass bulb gas cells before the measurements. The temperature is maintained constant (298 K) by placing the samples in an external water bath during the measurements.

### **EPR measurements**

Continuous wave (CW) X-band (9.4 GHz) EPR spectra were collected on a Bruker Magnettech ESR5000 spectrometer with a modulation frequency of 100 kHz. Field sweep echo-detected spectra were recorded on a Bruker ELEXYS E-580 spectrometer operating at Q-band (34.2 GHz) fitted with a Q-band resonator (EN-5107-D2). Temperature was controlled by an Oxford Instruments CF935 continuous flow cryostat using liquid helium. The activated samples were packed into capillaries and sealed with epoxy glue (EPOXIES) inside an Ar-filled glovebox.

### **NMR measurements**

NMR experiments were carried out on a Bruker 9.4T Avance Neo spectrometer equipped with a sweep coil and a 263 GHz gyrotron. Solid-state  $^1\text{H}$  NMR spectra were recorded at room temperature using 1.3 mm probe at a MAS frequency of 60 kHz. A rotor-synchronized Hahn-echo detection with the nutation frequency of 114 kHz was utilized. DNP experiments were performed using a 3.2 mm double resonance low temperature (LT)-DNP probe. The activated samples were packed into 3.2 mm sapphire MAS-DNP rotors and sealed with a Teflon plug and a zirconia cap inside an Ar-filled glovebox. Rotors were quickly inserted into the probe and spun at 9 kHz with dry  $\text{N}_2$ . The sample temperature was ca. 98 and 110 K without and with microwave irradiation, respectively.  $^1\text{H}$  spectra were measured using a rotor-synchronized Hahn-echo sequence following a train of 20 saturation pulses separated by 1 ms delays and a delay for relaxation or polarization build-up. The nutation frequency of all pulses was 80 kHz. Direct-polarization  $^{13}\text{C}$  MAS NMR spectra were recorded with  $^1\text{H}$  decoupling following a train of 20 saturation pulses separated by 1 ms delay and a delay for relaxation or polarization build-up. Enhancement factors were determined from the ratio between the integrated area of the spectra acquired with and without microwaves, and the errors were propagated from the signal to noise ratio. The nutation frequencies were 102, 125, and 74 kHz for  $^{13}\text{C}$  saturation,  $^{13}\text{C}$  excitation and  $^1\text{H}$  decoupling pulses, respectively.  $^1\text{H}$ - $^{13}\text{C}$  cross-polarization (CP) MAS experiments were initialized by a train of 20 saturation pulses with 70 kHz amplitude separated by 1 ms delay. During the contact time, the nutation frequencies for  $^{13}\text{C}$  and  $^1\text{H}$  were 51 kHz and 60 kHz, respectively.  $T_1$  relaxation and DNP build up times were measured using a saturation recovery sequence. A MATLAB code was used to fit the obtained data with stretched exponential function and the errors in the fit values were taken as one standard deviation of the fit.

### **“Freeze-thaw” protocol**

To remove  $\text{O}_2$  for Gd-LaBTB samples, the 3.2 mm sapphire rotor was inserted and spun inside the LT-DNP probe for nearly 15 min, cooling the sample down to ca. 100 K. Then the sample was ejected from the stator and kept in the insert/eject holder at the bottom of the probe at close to ambient temperature for 5 min (unless stated otherwise).

During this time, the probe stator was kept at ca. 100 K by flushing it with maximal flow of bearing, drive and VT. After that, the rotor was inserted back into the DNP probe stator and spun to perform DNP measurements.

### Additional experimental data

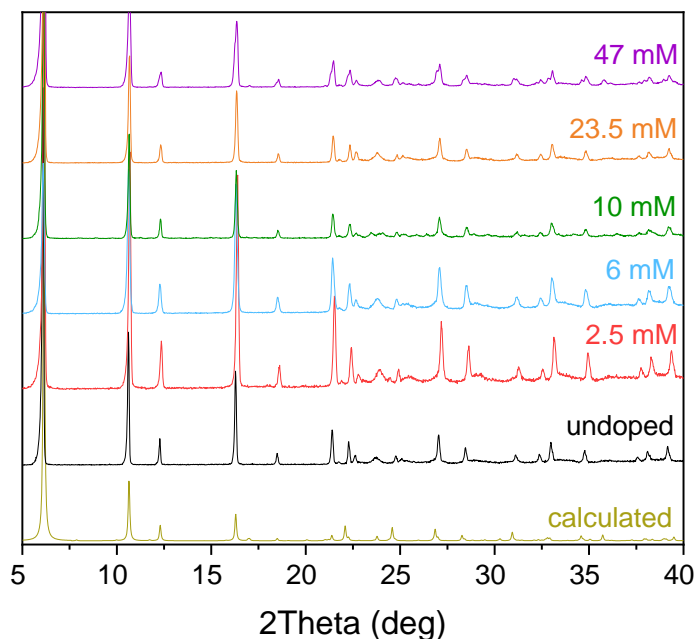


**Figure S1.** X-ray diffraction patterns acquired for as-synthesized samples: undoped LaBTB (black) and Gd-doped LaBTB with 2.5 (red), 6 (blue), 10 (green), 23.5 (orange) and 47 mM (purple) Gd(III). Calculated diffraction pattern (gold) was generated in Mercury software © using \*.cif file from CCDC database (# 9049974).

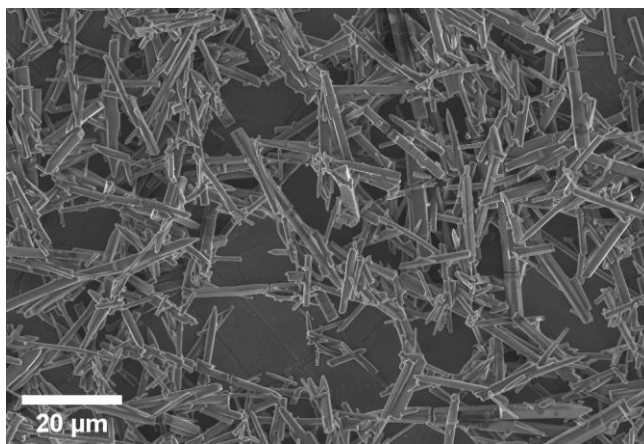


**Figure S2.** SEM image of as-synthesized Gd-LaBTB sample with 47 mM Gd(III) concentration (scale bar 20 μm).

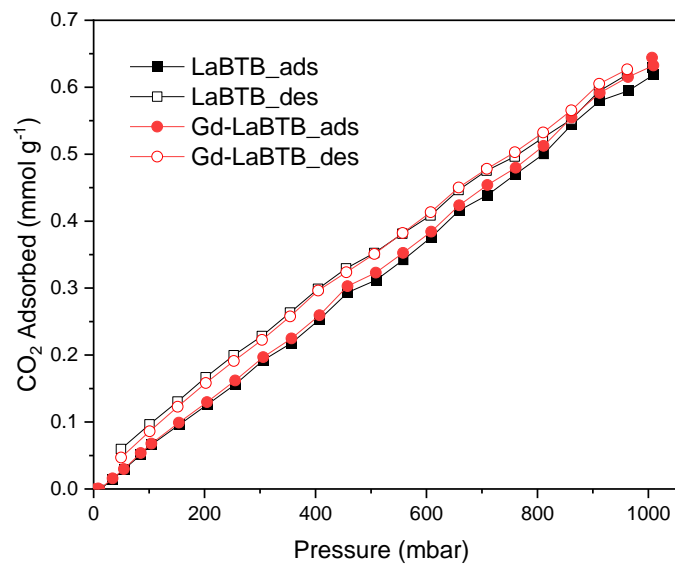


**Figure S3.** CO<sub>2</sub> adsorption (filled symbols) and desorption (open symbols) isotherms measured for the undoped LaBTB (black squares) and 23.5 mM Gd-LaBTB (red circles) samples at 298 K.

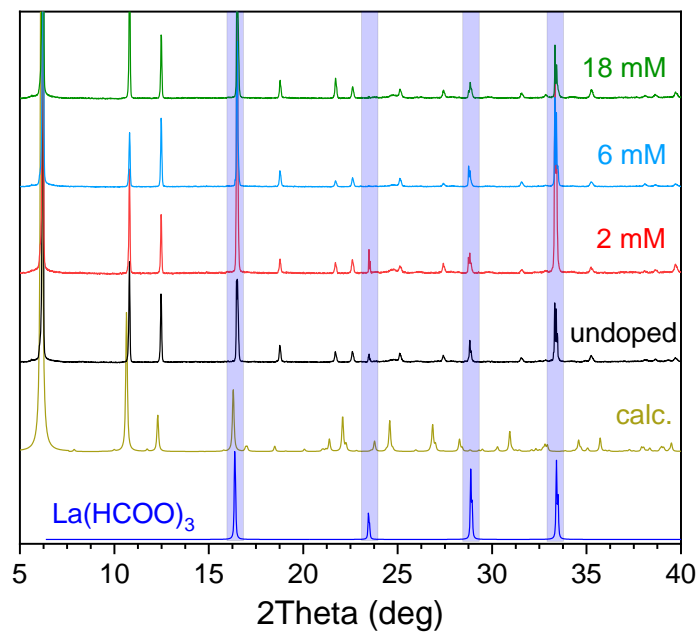


**Figure S4.** X-ray diffraction patterns acquired for samples synthesized using an alternative procedure described by Kitagawa and co-workers:<sup>2</sup> undoped LaBTB (black) and Gd-doped LaBTB with 2 (red), 6 (light blue) and 18 mM (green) Gd(III). Concentrations are calculated based on Gd loading. Measurements were carried out under Ar atmosphere after activation of samples at 423 K in vacuum. Blue areas indicate reflections corresponding to lanthanum formate phase. Calculated diffraction pattern for LaBTB (gold) was generated in Mercury software © using \*.cif file from CCDC database (# 9049974). Calculated diffraction pattern for lanthanum formate  $\text{La}(\text{HCOO})_3$  (dark blue) was obtained from ICDD database (# 00-018-0674).

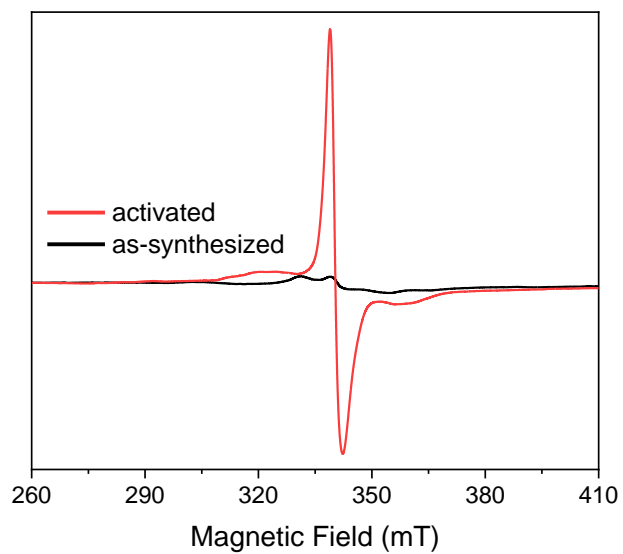


**Figure S5.** CW-EPR spectra of the 47 mM Gd-LaBTB sample measured at 9.4 GHz (X-band) at 100 K: as-synthesized (black) and activated at 423 K in vacuum (red). Activated material was measured under Ar.

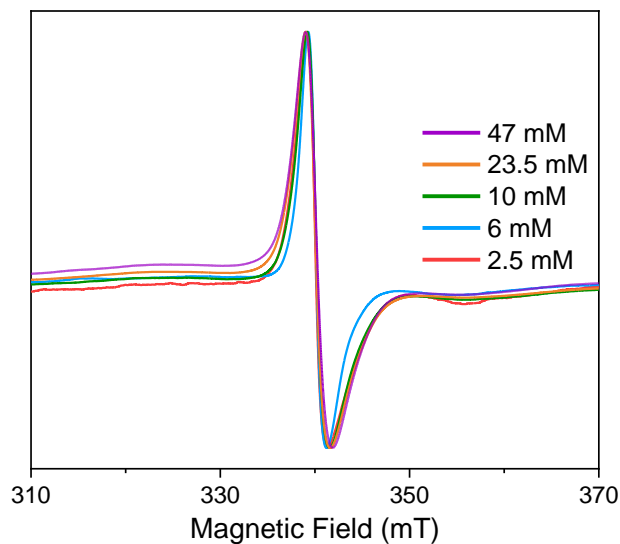


**Figure S6.** Normalized CW-EPR spectra of the Gd-LaBTB samples with 2.5 (red), 6 (blue), 10 (green), 23.5 (orange), 47 mM (purple) Gd(III) measured at 9.4 GHz (X-band) at 100 K. Samples were activated at 423 K in vacuum and packed under Ar.

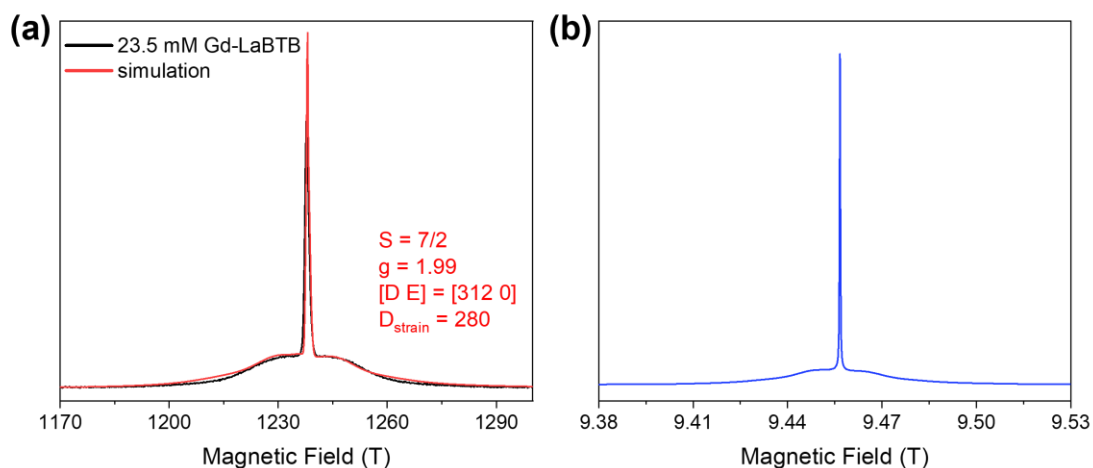


**Figure S7.** a) Field-sweep echo detected EPR spectrum of 23.5 mM Gd-LaBTB sample (black) acquired at 34.2 GHz (Q-band) at 100 K and simulated EPR spectrum (red) with parameters shown in red. Note that a simple isotropic model was exploited for fitting the spectra that does not consider the effect of remaining mobility of the Gd-LaBTB sample at 100K. Sample was activated at 423 K in vacuum and packed under Ar. b) Simulated EPR spectrum at 9.4 T and electron frequency of 263.5 GHz. Parameters from (a) were used to simulate the spectrum.

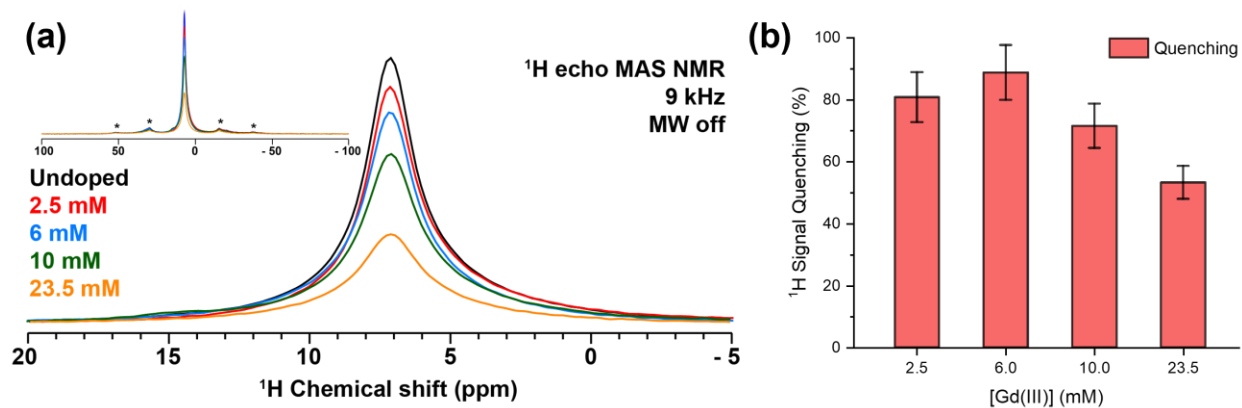


**Figure S8.** a)  $^1\text{H}$  MAS NMR spectra of undoped LaBTB (black) and Gd-doped LaBTB samples with 2.5 (red), 6 (blue), 10 (green) and 23.5 (orange) mM Gd(III) acquired at 100 K and 9 kHz MAS. Samples were stabilized until constant  $T_1(^1\text{H})$  without “freeze-thaw” cycles. The inset shows the same spectra with broad spectral width, with no additional signals for Gd-doped samples detected; b)  $^1\text{H}$  signal quenching (with  $\text{O}_2$ ) as a function of Gd(III) concentration in Gd-LaBTB samples. Quenching (in %) is defined as a ratio between NMR signal area of a doped and an undoped sample.

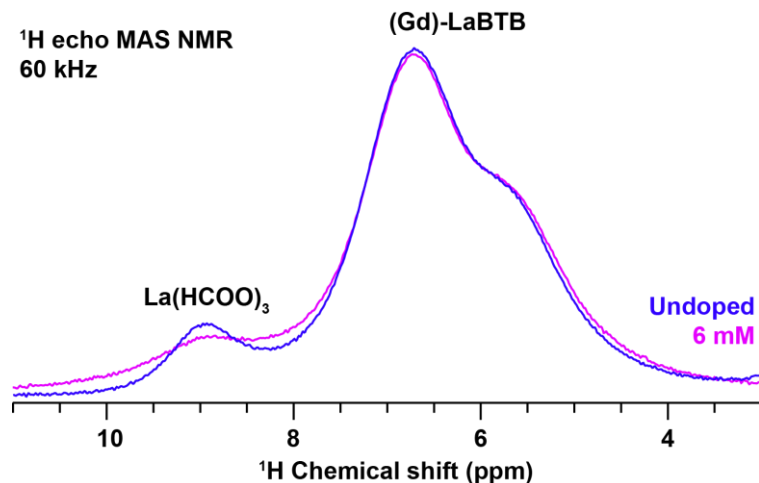


**Figure S9.**  $^1\text{H}$  MAS NMR spectrum of undoped LaBTB (blue) and 6mM Gd-doped LaBTB (magenta) samples acquired at ambient temperature and 60 kHz MAS. The samples contain lanthanum formate  $\text{La}(\text{HCOO})_3$  impurity phase exhibiting  $^1\text{H}$  resonance at ca. 9 ppm.

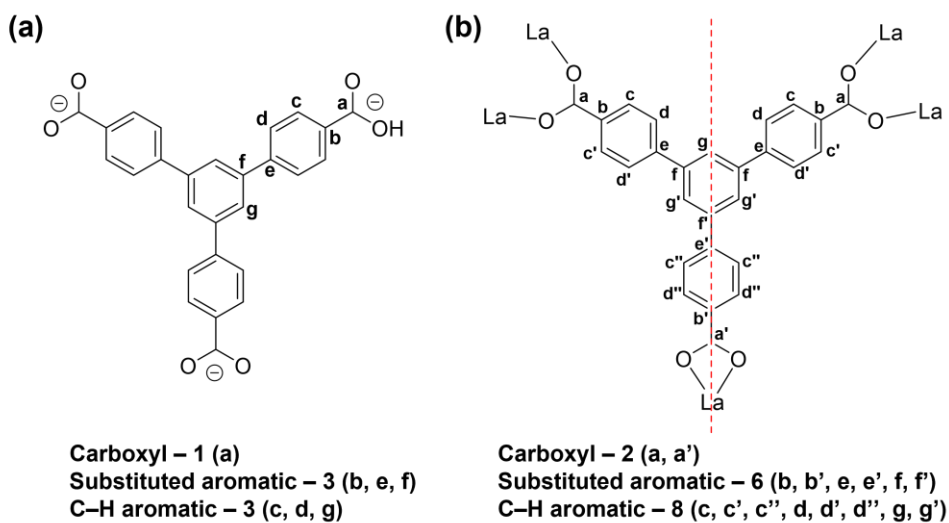


**Figure S10.** a) Molecular structure of  $\text{BTB}^{3-}$  linker. Chemically non-equivalent  $^{13}\text{C}$  nuclei, expected to have different chemical shifts, are labeled with different letters; b)  $\text{La}(\text{III})\text{-BTB}^{3-}$  connectivity in the crystal structure of LaBTB (see ref. 2). Crystallographically non-equivalent  $^{13}\text{C}$  nuclei are labeled with different letters, with 0, 1, or 2 apostrophe symbols. Red dashed line indicates a plane of symmetry. Below the structures, the non-equivalent carbon nuclei are split into groups based on their functionality – carboxyl, substituted and non-substituted C–H aromatic carbons.

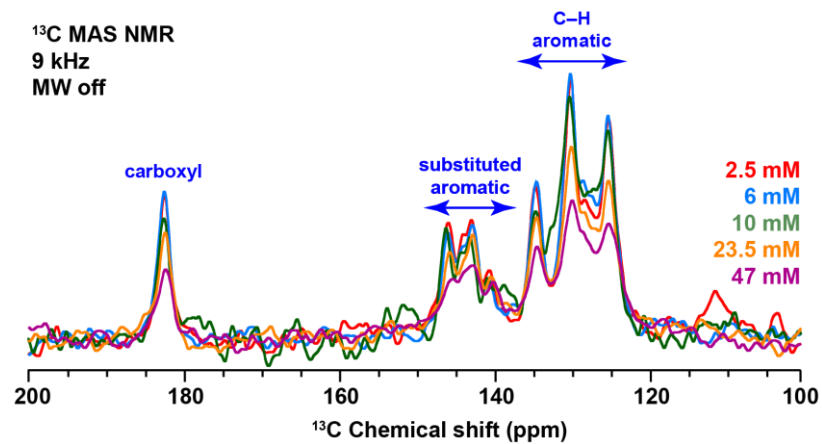


**Figure S11.** <sup>13</sup>C MAS NMR spectra of Gd-doped LaBTB samples with 2 (red), 6 (blue), 10 (green), 23.5 (orange) and 47 (purple) mM acquired at 100 K and 9 kHz MAS. Prior to measurements, samples were subjected to two “freeze-thaw” cycles to remove O<sub>2</sub>.

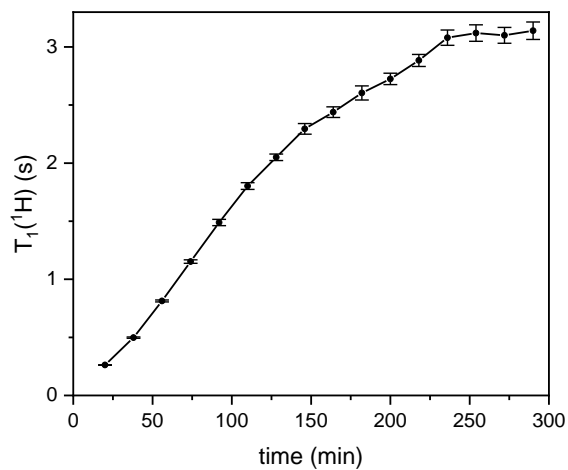


**Figure S12.** <sup>1</sup>H relaxation time  $T_1$  as a function of time from insertion of the 6 mM Gd-LaBTB sample into the cold (ca. 100 K) LT-DNP probe. Throughout the experiment the microwave source was on.

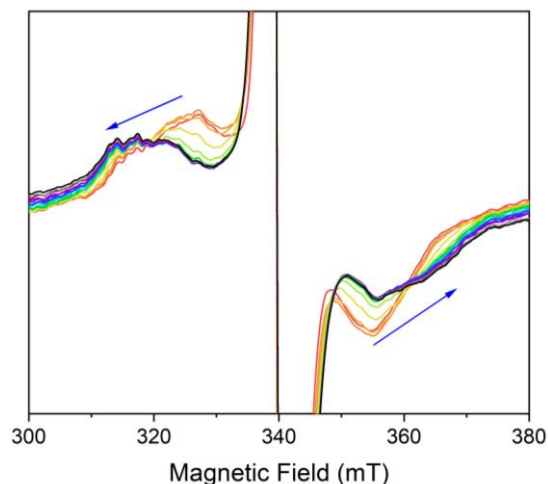


**Figure S13.** CW-EPR spectra of the 6 mM Gd-LaBTB sample recorded every 10 min on X-band at 100 K. The side lines corresponding to Gd(III) ZFS satellite transitions are zoomed in. Blue arrows indicate the changes with time.

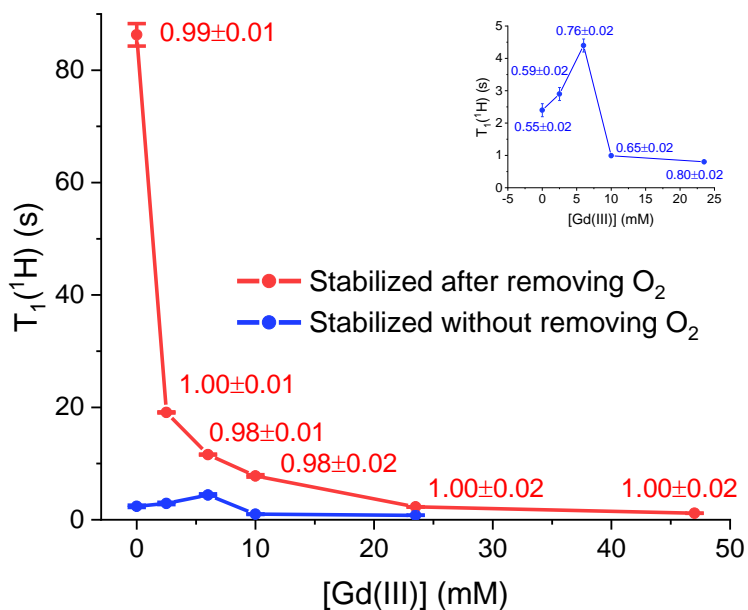


**Figure S14.**  $^1\text{H}$  nuclear relaxation time  $T_1(^1\text{H})$  for Gd-LaBTB samples at 100 K as a function of the Gd(III) concentration. Samples were stabilized until constant  $T_1(^1\text{H})$  either without removing  $\text{O}_2$  (blue) or after  $\text{O}_2$  was removed using the “freeze-thaw” procedure (red). The inset shows the magnified region for  $\text{O}_2$  containing samples.  $T_1(^1\text{H})$  values were obtained by fitting saturation recovery curves with the stretched exponential function:  $I(t) = I_0(1 - \exp[-(\tau/T_1)^\beta])$ . The obtained  $\beta$  values are shown next to the corresponding data points.

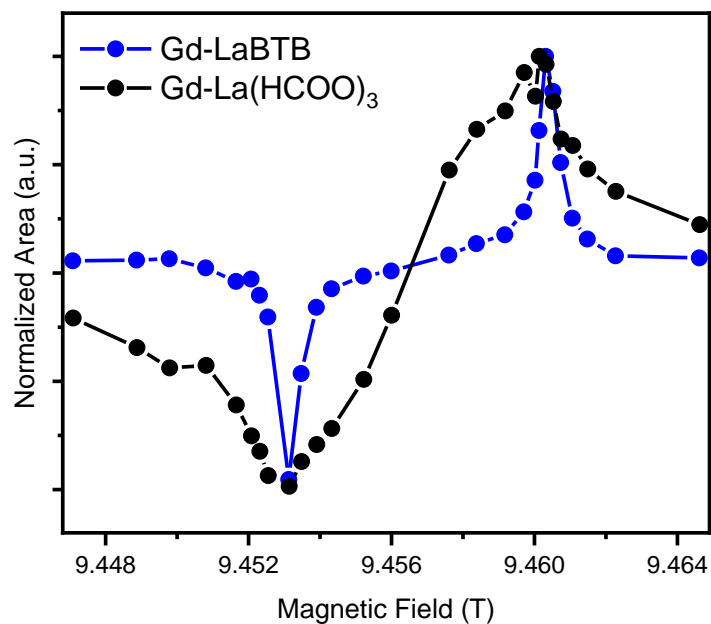


**Figure S15.** DNP field-sweep profiles obtained by integrating the  $^{13}\text{C}$  signals corresponding to the Gd-LaBTB (blue) and Gd-La(HCOO) $_3$  (black) phases that are present in the sample synthesized via modified procedure of Kitagawa and co-workers.<sup>2</sup> The target Gd(III) concentration was 6 mM. The sample was stabilized until a constant  $T_1(^1\text{H})$  without “freeze-thaw” cycles. Spectra were recorded with polarization times of 40 s.

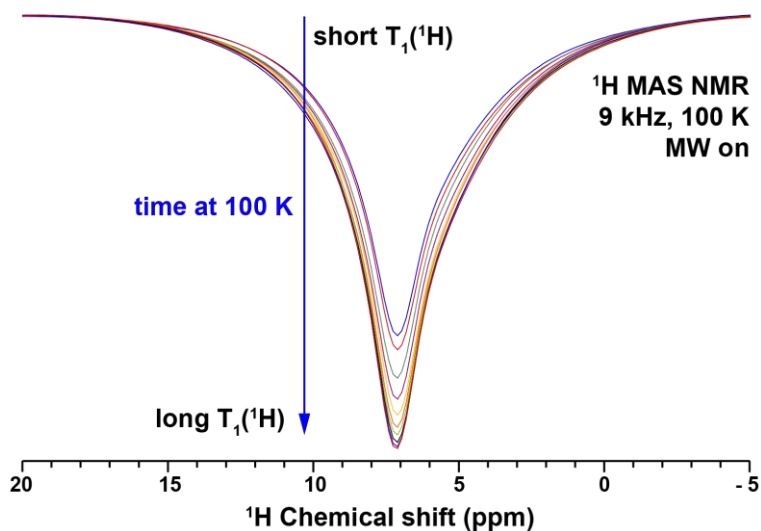


**Figure S16.**  $^1\text{H}$  single-pulse NMR spectra recorded for 2.5 mM Gd-LaLOF at 100K at the negative lobe of the  $^1\text{H}$  field-sweep profile with microwaves on. The sample was subjected to two 5 min “freeze-thaw” cycles until constant  $T_1(^1\text{H})$ , thawed for 30 mins, and then inserted back into the DNP probe stator kept at 100 K. From that point,  $^1\text{H}$  spectra were acquired every 16.7 min from top blue spectrum down to bottom red, as indicated by the blue arrow.

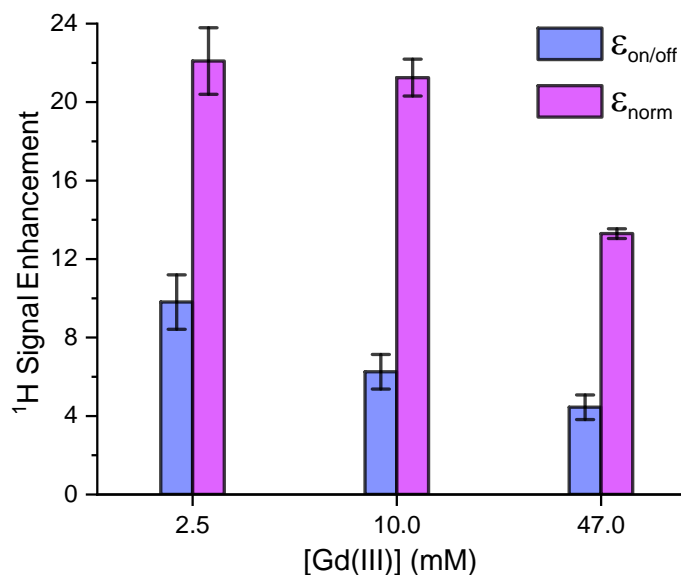


**Figure S17.** Enhancement factors for  $^1\text{H}$  nuclei as a function of Gd(III) concentration in Gd-LaBTB.  $\epsilon_{on/off}$  (blue) is determined as the ratio between integrated microwave-on and microwave-off signals at steady-state conditions ( $5T_{bu}$ );  $\epsilon_{norm}$  (magenta) is the enhancement  $\epsilon_{on/off}$  normalized by the paramagnetic quenching factors (see Figure S18) and the change in the build-time  $T_{bu}(^1\text{H})$  with respect to the relaxation time of the undoped LaBTB sample (Figure S19). All samples were subjected to two “freeze-thaw” cycles until constant  $T_1(^1\text{H})$ .

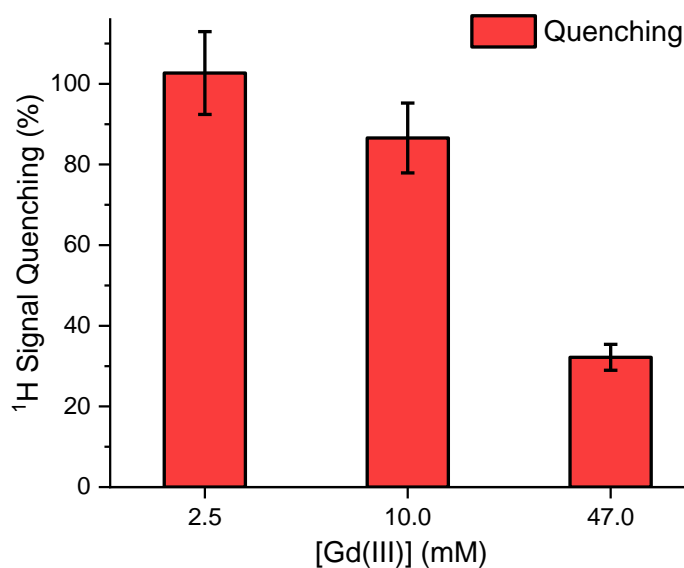


**Figure S18.**  $^1\text{H}$  signal quenching (without  $\text{O}_2$ ) as a function of the Gd(III) concentration in Gd-LaBTB samples at 100 K. Quenching (in %) is defined as a ratio between NMR signal area of a doped and an undoped sample. All samples were subjected to two “freeze-thaw” cycles until constant  $T_1(^1\text{H})$ .

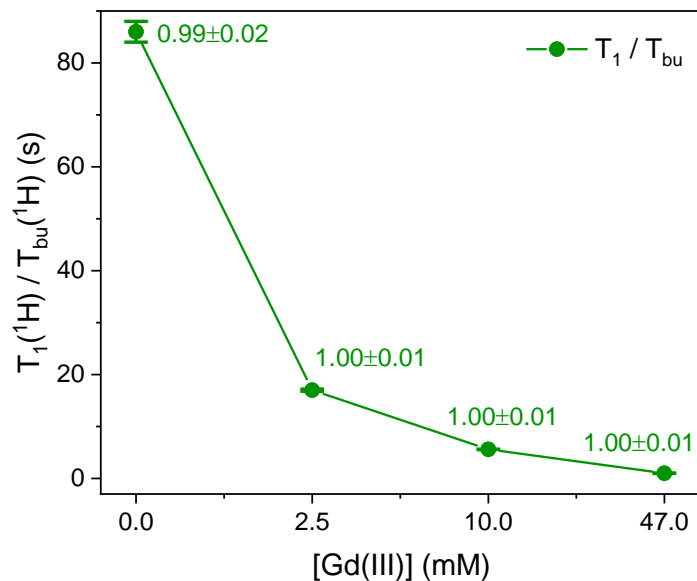


**Figure S19.**  $^1\text{H}$  nuclear relaxation time  $T_1(^1\text{H})$  for undoped LaBTB measured with microwaves off and build-up times  $T_{bu}(^1\text{H})$  for 2.5, 10 and 47 mM Gd-LaBTB samples measured with microwaves on. Measurements were performed at 100 K following two “freeze-thaw” cycles.  $T_1(^1\text{H})$  and  $T_{bu}(^1\text{H})$  values were obtained by fitting saturation recovery curves with the stretched exponential function:  $I(t) = I_0 \left( 1 - \exp[-(\tau/T_{\perp})^\beta] \right)$ . The obtained  $\beta$  values are shown next to the corresponding data points.

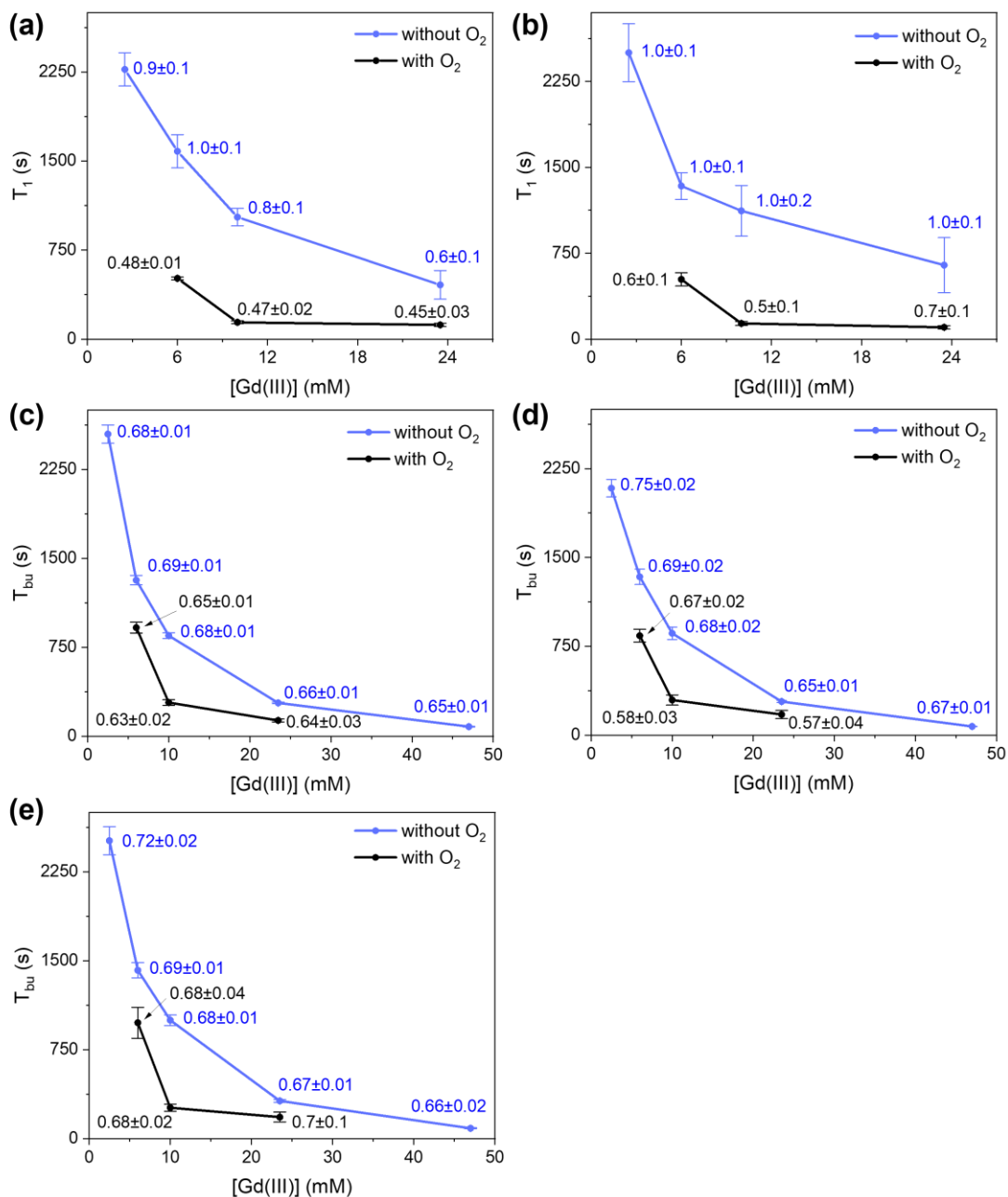


**Figure S20.**  $^{13}C$  nuclear relaxation time  $T_1(^{13}C)$  (a,b) and build-up time  $T_{bu}(^{13}C)$  (c,d,e) as a function of Gd(III) concentration in Gd-LaBTB for C-H aromatic (a,c), substituted aromatic (b,d), and carboxyl (e) carbon nuclei. Measurements were performed at 100 K after the stabilization of samples (until constant  $T_1(^1H)$ ) without (black) and with (blue) “freeze-thaw” cycles. Fitting was performed using stretched exponential function. The obtained  $\beta$  values are shown next to the corresponding data points. Note that due to low signal-to-noise ratio, we were not able to determine microwave-off  $T_1(^{13}C)$  values for 47 mM Gd-LaBTB sample as well as for carboxyl carbons in all samples.

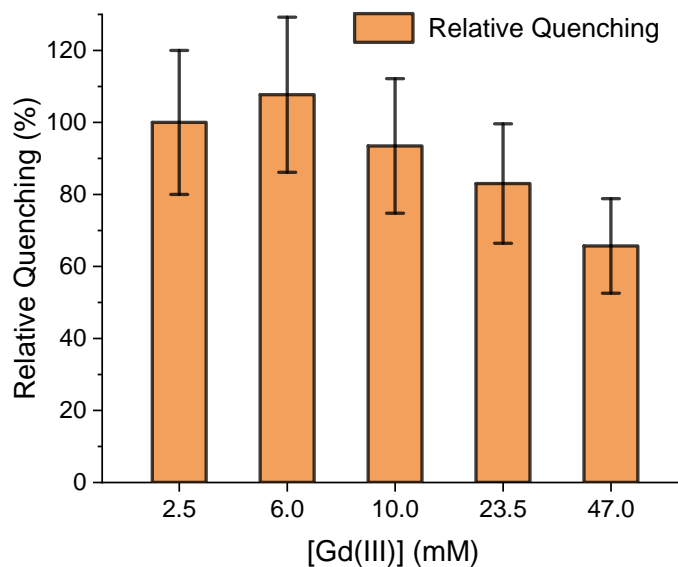


**Figure S21.**  $^{13}\text{C}$  signal quenching (without  $\text{O}_2$ ) as a function of the Gd(III) concentration in Gd-LaBTB samples at 100 K. Relative quenching (in %) is defined as a ratio between NMR signal area of a given sample and a 2.5 mM Gd-LaBTB sample, both recorded with microwaves off. All samples were subjected to two “freeze-thaw” cycles until constant  $T_1(^1\text{H})$ .

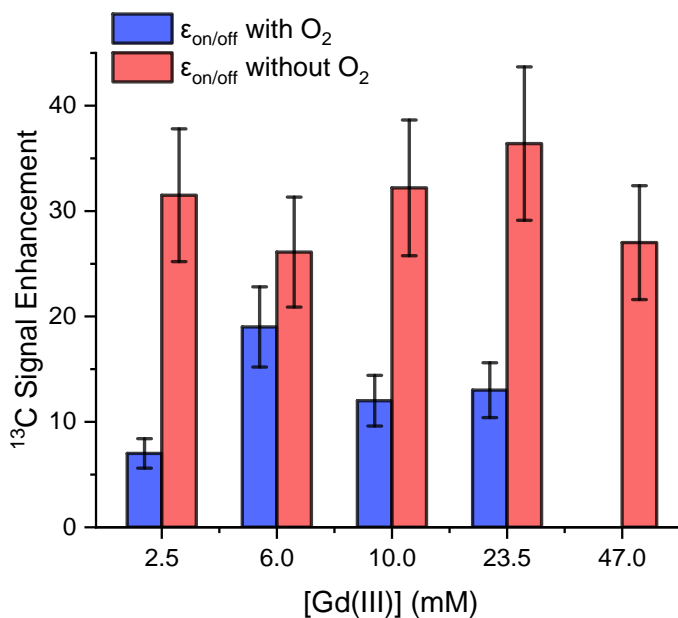


**Figure S22.** Enhancement factors for  $^{13}\text{C}$  nuclei as a function of Gd(III) concentration in Gd-LaBTB. The samples were either stabilized without “freeze-thaw” cycles (blue) or subjected to two “freeze-thaw” cycles (red) and then stabilized until constant  $T_1(^1\text{H})$ .  $\epsilon_{\text{on/off}}$  is determined as the ratio between integrated microwave-on and microwave-off signals at the steady-state conditions ( $5T_{\text{bu}}$ ).

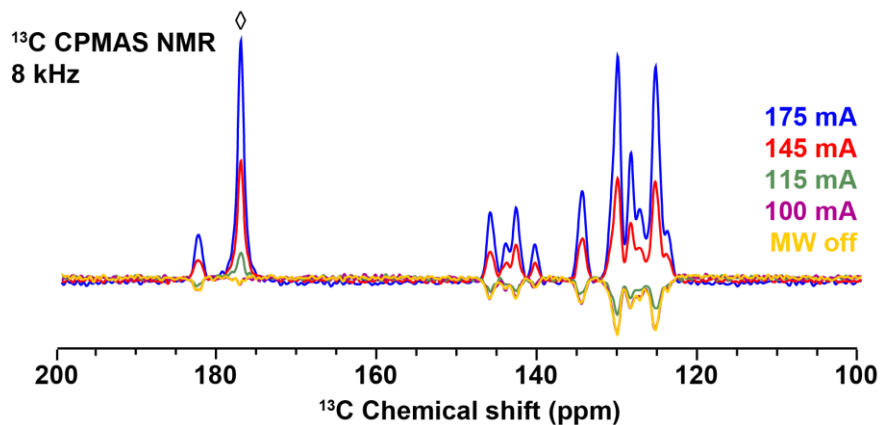


**Figure S23.**  $^1\text{H}$ - $^{13}\text{C}$  CPMAS NMR spectra of 6 mM Gd-doped LaBTB sample containing lanthanum formate impurity phase (labeled as  $\diamond$ ). The spectra were acquired at 100 K and 8 kHz MAS without microwaves (yellow) and with variable microwave power obtained by setting the current collector to 100 mA (purple), 115 mA (green), 145 mA (red), and 175 mA (blue). The field position corresponds to the negative lobe in the  $^1\text{H}$  field-sweep profile, and the phase was set negative for the microwave-off spectrum.

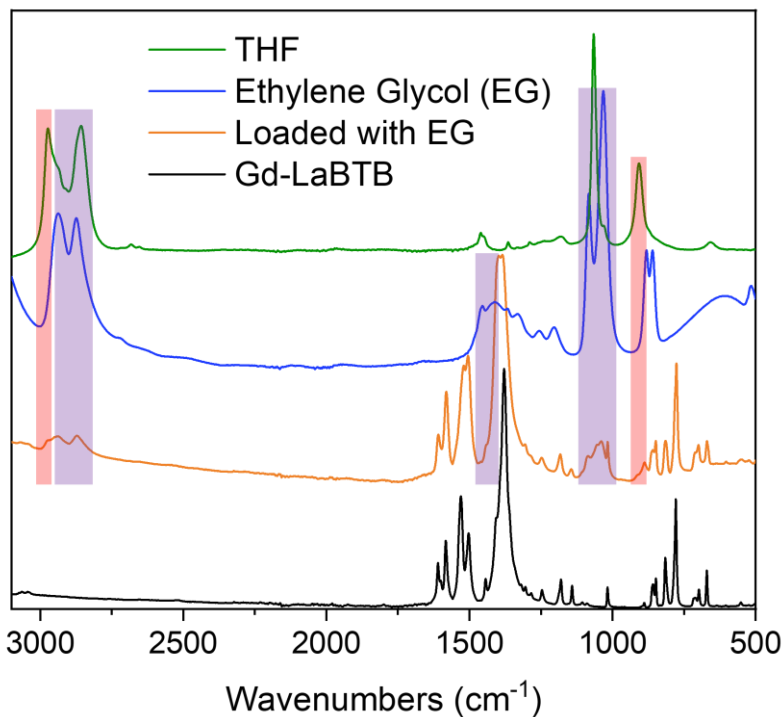


**Figure S24.** Attenuated total reflection infrared (ATR IR) spectra of the activated 23.5 mM Gd-doped LaBTB before (black) and after (orange) loading of the ethylene glycol (EG) guest molecule; neat ethylene glycol (blue) and neat THF (green). The MOF samples were stored in the Ar-filled glovebox and exposed to air 5 mins prior to

measurements. Vertical lines indicate absorption bands present in the spectra of a neat EG (purple) and THF (red) and observed in the EG-loaded Gd-LaBTB.

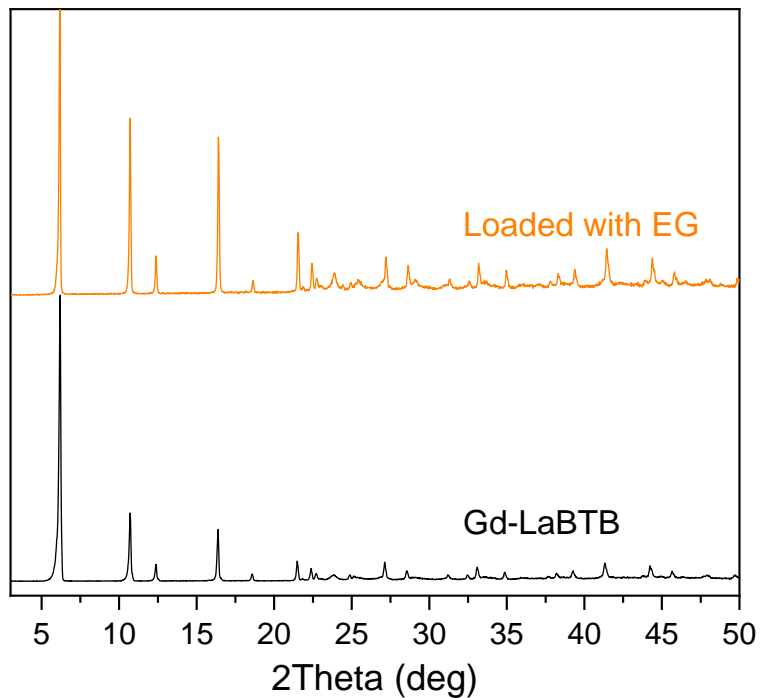


**Figure S25.** X-ray diffraction patterns acquired for the activated Gd-doped LaBTB sample with 23.5 mM Gd(III) before (black) and after (orange) the sample was loaded with the ethylene glycol (EG) guest molecule. The samples were stored in the Ar-filled glovebox and exposed to air 5 mins prior to measurements.

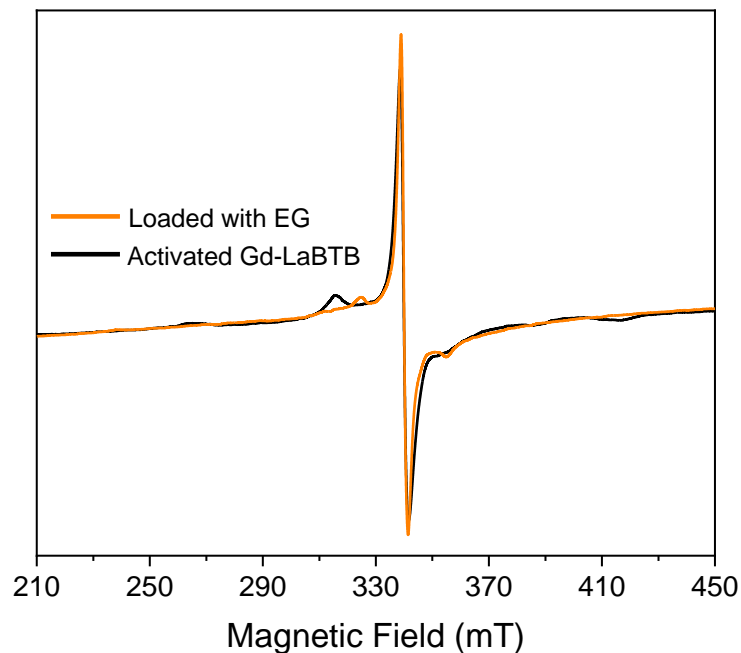


**Figure S26.** CW-EPR spectra of the activated 23.5 mM Gd-LaBTB sample measured at 9.4 GHz (X-band) at 100 K: before (black) and after (orange) loading of the ethylene glycol (EG) guest molecule. The samples were measured under Ar.

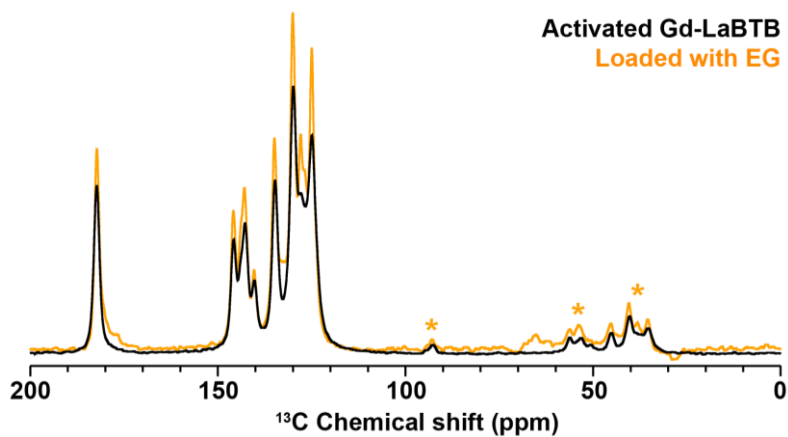


**Figure S27.** <sup>13</sup>C MAS NMR spectra of the activated 23.5 mM Gd-doped LaBTB sample before (black) and after (orange) loading of the ethylene glycol (EG) guest molecule. The spectra were acquired at 100 K and 9 kHz MAS with microwaves on. Prior to measurements, samples were subjected to two “freeze-thaw” cycles to remove O<sub>2</sub>. Asterisks mark spinning sidebands.

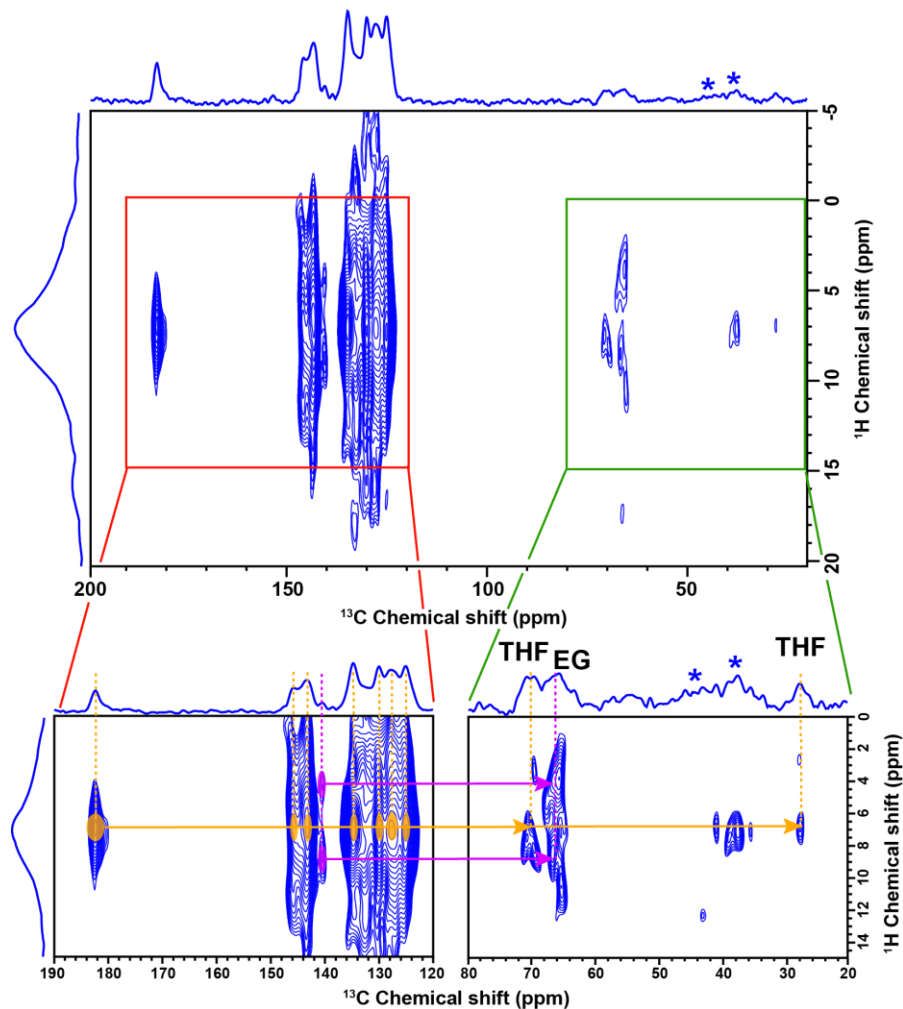


**Figure S28.**  $^1\text{H}$ - $^{13}\text{C}$  HETCOR experiment of the activated 23.5 mM Gd-LaBTB sample loaded with the ethylene glycol (EG) guest molecule, collected at 100 K. The CP contact time was 2 ms. 60 indirect increments and 200 transients were accumulated with a relaxation delay of 3 s. Top: overview spectrum. Bottom: zoom-in of the  $^{13}\text{C}$  aromatic region with MOF signals (left) and  $^{13}\text{C}$  aliphatic region with THF and EG signals (right). Ellipsoids and arrows indicate polarization transfer from  $^1\text{H}$  nuclei in Gd-LaBTB framework to  $^{13}\text{C}$  nuclei in THF (orange) and EG (purple).

**Table S1.** Results of X-ray fluorescence (XRF) analysis on Gd-LaBTB samples: target Gd(III) concentration –  $[\text{Gd(III)}]_{\text{target}}$  – calculated based on Gd(III) loading; ratio between areas under La and Gd peaks in XRF spectra –  $(\text{La}/\text{Gd})_{\text{XRF}}$ ; Gd(III) concentration found by XRF analysis –  $[\text{Gd(III)}]_{\text{XRF}}$  – calculated based on  $(\text{La}/\text{Gd})_{\text{XRF}}$

$[\text{Gd(III)}]_{\text{target}}$ , mM	$(\text{La}/\text{Gd})_{\text{XRF}}$	$[\text{Gd(III)}]_{\text{XRF}}$ , mM
28	35.9±0.4	46.7±0.5
14	70±2	23.5±0.5
7	168±12	10±1
3.5	290±38	6±1
1.75	530±123	2.5±0.5

**Table S2.** DNP enhancement of individual  $^{13}\text{C}$  NMR signals of Gd-LaBTB samples: concentration of Gd(III) in the sample as determined by XRF –  $[\text{Gd(III)}]$

$[\text{Gd(III)}]$	$^{13}\text{C}$ Chemical Shift, ppm										
	182.4	145.7	144.0	142.4	140.2	134.1	129.8	128.1	126.9	124.9	123.5
2.5	5±1 <sup>a</sup>	7±1	9±2	7±1	6±1	8±2	7±1	8±2	6±1	6±1	5±1
6	17±3	22±4	22±4	14±3	33±7	20±4	19±4	22±4	13±3	15±3	15±3
10	14±3	11±2	14±3	14±3	12±2	13±3	10±2	9±2	9±2	9±2	14±3
23.5	15±3	7±1	14±3	8±2	30±6	15±3	9±2	14±3	10±2	9±2	8±2

<sup>a</sup> DNP enhancement defined as a ratio of NMR signal area with microwaves on and off.

**Table S3.** MIDNP enhancement factors reported in the literature: material; hyperpolarized nuclei; gyromagnetic ratio  $|\gamma_n|$  of the hyperpolarized nuclei; the highest achieved microwave-on/off signal enhancement –  $|\epsilon_{\text{top}}|$ ; theoretical enhancement –  $|\epsilon_{\text{theor}}|$  – calculated as a ratio of the electron and the nuclear gyromagnetic ratios; percentage of the theoretical enhancement achieved in the experiment; reference.

Material	Nucleus	$ \gamma_n $ , MHz T <sup>-1</sup>	$ \epsilon_{\text{top}} $	$ \epsilon_{\text{theor}} $	$\epsilon_{\text{top}}/\epsilon_{\text{theor}}$ , %	Reference
(Y,Gd)-CeO <sub>2</sub>	<sup>89</sup> Y	2.095	193	13377	1.4 %	3
Gd(tpatcn)	<sup>13</sup> C	10.708	122	2617	4.7 %	4
Gd-CeO <sub>2</sub>	<sup>17</sup> O	5.772	652	4855	13.4 %	5
Gd-Li <sub>2</sub> CaSiO <sub>4</sub>	<sup>29</sup> Si	8.465	113	3311	3.6 %	6
Gd-LaBTB	<sup>13</sup> C	10.708	36	2617	1.4 %	This work

**Table S4.** Estimated  $^1\text{H}$ - $^1\text{H}$  spin diffusion lengths for undoped and Gd-doped LaBTB samples with 2.5, 10 and 47 mM Gd(III). The spin diffusion coefficient ( $D$ ) was estimated following van der Wel et al.<sup>7</sup> as  $D = \pi d^2 \omega_d^2 / \omega_r$ , where  $d$  is the  $^1\text{H}$  internuclear average distance,  $\omega_d$  the strength of the dipolar interaction (for simplicity calculated for an

averaged distance) and  $\omega_r$  is the MAS frequency. The diffusion length is estimated as  $L = \sqrt{DT_1}$ , where the estimated diffusion coefficient  $D$  is used with the longitudinal relaxation of protons ( $T_1$ ) measured at 100 K and 9 kHz MAS rate. We note that these values are likely an overestimation of the diffusion length scale and the diffusion rate as the dipolar interaction will be averaged by the dynamics in the framework. These values are compared with the average distance between Gd(III) dopants.<sup>8</sup>

<b>[Gd(III)], mM</b>	<b><math>T_1(^1\text{H})</math>, s</b>	<b>L, nm</b>	<b>Average Gd distance, nm</b>
0	86	147	-
2.5	17	65	10.8
10	5.6	38	6.8
47	1	16	4

## References

- 1 T. Devic, V. Wagner, N. Guillou, A. Vimont, M. Haouas, M. Pascolini, C. Serre, J. Marrot, M. Daturi, F. Taulelle and G. Férey, *Microporous Mesoporous Mater.*, 2011, **140**, 25–33.
- 2 J. Duan, M. Higuchi, S. Horike, M. L. Foo, K. P. Rao, Y. Inubushi, T. Fukushima and S. Kitagawa, *Adv. Funct. Mater.*, 2013, **23**, 3525–3530.
- 3 D. Jardón-Álvarez, N. Kahn, L. Houben and M. Leskes, *J. Phys. Chem. Lett.*, 2021, **12**, 2964–2969.
- 4 G. Stevanato, D. J. Kubicki, G. Menzildjian, A.-S. Chauvin, K. Keller, M. Yulikov, G. Jeschke, M. Mazzanti and L. Emsley, *J. Am. Chem. Soc.*, 2019, **141**, 8746–8751.
- 5 M. A. Hope, S. Björgvinsdóttir, D. M. Halat, G. Menzildjian, Z. Wang, B. Zhang, J. L. MacManus-Driscoll, A. Lesage, M. Lelli, L. Emsley and C. P. Grey, *J. Phys. Chem. C*, 2021, **125**, 18799–18809.
- 6 B. Thomas, D. Jardón-Álvarez, R. Carmieli, J. van Tol and M. Leskes, *J. Phys. Chem. C*, 2023, **127**, 4759–4772.
- 7 P. C. A. van der Wel, K.-N. Hu, J. Lewandowski and R. G. Griffin, *J. Am. Chem. Soc.*, 2006, **128**, 10840–10846.
- 8 D. Jardón-Álvarez and M. Leskes, in *Reference Module in Chemistry, Molecular Sciences and Chemical Engineering*, Elsevier Inc, 2021.